Article

Aspartame as a Green and Effective Corrosion Inhibitor for T95 Carbon Steel in 15 wt.% HCl Solution

Ifeanyi E. Uzoma [1], Moses M. Solomon [1,*], Roland T. Loto [2] and Saviour A. Umoren [3]

[1]   Department of Chemistry, College of Science and Technology, Covenant University, Ota 112104, Nigeria;
     ifeanyiuzo5@gmail.com
[2]   Department of Mechanical Engineering, Covenant University, Ota 112104, Nigeria; toluloto@gmail.com
[3]   Interdisciplinary Research Center for Advanced Materials, King Fahd University of Petroleum and Minerals,
     Dhahran 31261, Saudi Arabia; umoren@kfupm.edu.sa
*   Correspondence: moses.solomon@covenantuniversity.edu.ng

Abstract: Oil well acidizing, although a stimulation process, induces the corrosion of metallic equipment and well tubing. There is, at present, a high demand for effective and less toxic high-temperature corrosion inhibitors for the acidizing process due to the failing of the existing inhibitors at high temperatures occasioned by increases in the well depths. In this study, aspartame (ASP), a commercially available natural compound, is examined as a corrosion inhibitor for T95 carbon steel in 15 wt.% HCl solution at 60, 70, 80, and 90 °C using the weight loss, electrochemical impedance spectroscopy (EIS), potentiodynamic polarization (PDP), scanning electron microscope (SEM), energy dispersive spectroscopy (EDX), and optical profilometry (OP) techniques. It was found that ASP possesses a corrosion inhibiting effect at the studied conditions. Inhibition efficiency increased with increases in temperature. With 2000 ppm ASP, inhibition efficiency of 86% was achieved from the weight loss method at 90 °C after 4 h of immersion. Results from the electrochemical techniques are in good agreement with the weight loss results. PDP results reveal that ASP acted as a mixed-type corrosion inhibitor under the investigated conditions. The inhibition ability of ASP is due to adsorption on the steel surface and has been confirmed by the SEM, OP, and EDX results. ASP is a promising active compound for the formulation of acidizing corrosion inhibitors.

Keywords: acidizing; corrosion; greenness; aspartame; adsorption

1. Introduction

Well stimulation is one aspect of oil and gas production development in the petroleum industry. The acidizing approach in well stimulation to activate the oil well reservoirs is one of numerous operational activities. It involves the injection of strong acids into the reservoir to dissolve soluble components or create wormhole channels to increase permeability and eliminate formation damage [1]. The acidizing process dissolves acid-soluble components inside underground rock formations and aids in the removal of material that has clogged the formation at the wellbore face, allowing more oil or gas to flow out of the production wells or to allow oil-displacing fluids to flow into injection wells [2,3]. The main goal of acidizing is to boost oil well fluid production by improving the drainage efficiency of the reservoir rock surrounding the wellbore. Strong acids, such as HCl, HF, HF mixes, and mild acids, such as acetic and formic acids, are frequently employed [4]. HCl is the most used acid in this technique since the reaction products are water-soluble. Typically, 15–28% HCl is used to finish the process [5]. The corrosion of structural materials exposed to acid occurs throughout these procedures. Mixing tanks, pipelines, casings, tubing, and storage facilities are examples of such materials, typically made of API-grade low-carbon steel because it is inexpensive and readily available [6]. Steel grade refers to the steel's yield strength. H-40, J-55, K-55, N-80, L-80, C-90, T-95, P-110, and Q-125 are the nine steel grade classifications. The letters denote the steel grade, which has nothing to do with the attributes, and the

number denotes the minimum yield strength. The higher the number, the greater the yield strength. Furthermore, the API standard divides the nine categories into four groups, with H, J, K, N in the first, L, C, T in the second, P in the third, and Q in the fourth. The steel grade in the first group has low strength. Grades L, C, and T denote limited-yield casing and tubing with anti-sulfur and anti-corrosive properties. L-80 is a restricted-yield tubing grade that comes in three varieties. L80-1, L80-9CR, and L80-13Cr are the three different types of L80. C-90 is a brand-new API grade that comes in two varieties: C90-1 and C90-2. In sour conditions, only C90-1 is recommended. This grade must be specially ordered, and it has been gradually phased out in favor of T-95. T-95 has high strength and is resistant to sulfide stress corrosion. However, it is not weight loss resistant. It also comes in two varieties: T95-1 and T95-2. The T95-2 variety is used in this work, and for convenience's sake, T95 shall be used henceforth.

Corrosion inhibitor technology is a practical, dependable, and cost-effective corrosion mitigation strategy [7–9]. Effective corrosion inhibitors must significantly reduce the rate of metallic corrosion during acidizing treatments. Corrosion inhibitors protect metal surfaces by adsorbing onto the surface through their active functionalities. The use of some natural compounds as corrosion inhibitors is motivated by the known dangers of most synthetic corrosion inhibitors. The traditional acidizing corrosion inhibitor, propargyl alcohol, according to the GHS classification, has a fatal dose (LD_{50}) of 20 mg/kg, an acute oral toxicity classification of category 3, and a chronic aquatic toxicity rating of category 2 [10–12]; hence, it is short of the PARCOM requirement for environmentally benign chemicals [13,14]. From the standpoint of environmental compatibility, the area of corrosion inhibitors is undergoing dramatic changes as environmental organizations in various countries have imposed rigorous standards and restrictions on the use and release of corrosion inhibitors. As a result, developing novel corrosion inhibitors with little or no adverse effects has been deemed more vital. Green corrosion inhibitors are from a variety of natural sources. They have many polar atoms and electron-rich linkages, making them rich in organic molecules [1].

In addition to the clarion call for green chemicals, the recent depletion of shallower oil wells is pushing offshore oil and gas drilling activities to move further offshore and deeper underwater so as to find sources of production in low-risk areas. Meanwhile, this poses a serious challenge to the industry because of the higher temperature and pressure as the well gets deeper. The implication is that most of the effective inhibitors for the acidizing process are losing their potency. Most often, the inhibition efficiency of organic inhibitors [7], including plant extracts [15–17], decreases with increases in temperature. There is, therefore, a high demand for corrosion inhibitors that can perform effectively at high temperatures.

This study aims to create a low-cost, effective, and environmentally acceptable corrosion inhibitor for use in high-temperature acidizing processes. Aspartame, (*N*-(L-α-Aspartyl)-L-phenylalanine) was tested as a corrosion inhibitor for API T95 carbon steel in a 15 wt.% HCl solution. Aspartic acid and phenylalanine (amino acids) are two components of aspartame. It has an LD_{50} oral value of >10,000 mg/kg [18]. It is also very cheap and cost-effective. Figure 1 shows the chemical structure of aspartame. The examination included a variety of methods, including weight loss, electrochemical methods (electrochemical impedance spectroscopy and potentiodynamic polarization), and surface characterization (by scanning electron microscope (SEM) and optical profilometer (OP)).
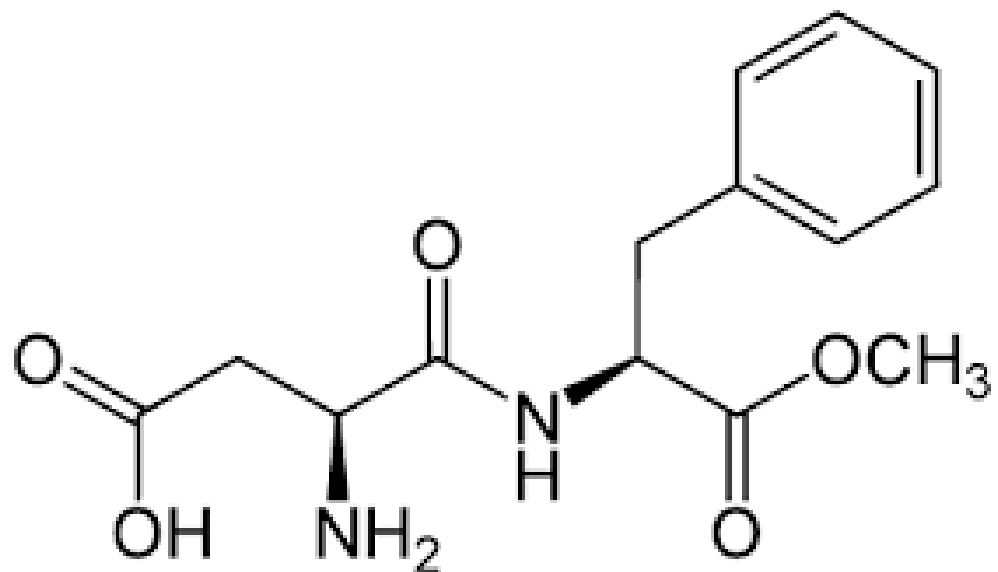
Figure 1. Chemical structure of Aspartame [19].

2. Materials and Methods

2.1. Materials, Sample Preparation, and Chemicals

The steel material used for this research is a pipe material, i.e., carbon steel material; more precisely, it is a T95 steel of chemical composition in wt.% (C:0.45, P:0.030, Mo:0.85, Si:0.45, S:0.010, Cr:1.50, Mn:1.20, Ni:0.99, and the balance Fe). For the weight loss experiments, the metal was cut into samples with surface areas of 12 cm^2. Samples for electrochemical tests had surface areas of 1 cm^2 and were soldered to a copper wire and abraded with Emery paper from 60 to 800 grits. The samples were thoroughly cleaned with distilled water, degreased with acetone, and dried at room temperature in a desiccator before being mounted using VersoCit-2 epoxy resin (Struers' product). The corrodent, 15 wt.% hydrochloric acid, was prepared by diluting 37% concentrated HCl with distilled water. Aspartame (ASP) was purchased from Sigma-Aldrich, CAS No: 22839-47-0. The stock solution of the ASP inhibitor (100,000 ppm) was prepared by dissolving appropriate amount in 20 mL ethanol/water 1:1 ratio mixture. The required concentrations (500–2000 ppm) were obtained by diluting the stock solution with 15 wt.% HCl solution.

2.2. Weight Loss Measurements

Before weight loss testing, the samples were mechanically abraded with Emery paper from 60 to 800 grits. The samples were thoroughly cleaned with distilled water, degreased with acetone, and dried at room temperature in a desiccator. The initial weight of the samples was noted and recorded. The pre-weighed samples in triplicate were submerged in a 15 wt.% HCl solution without and with various inhibitor concentrations (500 ppm, 1000 ppm, 1500 ppm, and 2000 ppm) at several temperatures (60 °C, 70 °C, 80 °C, and 90 °C) for 4 h. After the immersion process, the samples were removed, cooled to room temperature, dipped in a pickling solution (zinc dust + NaOH solution) for 1 min, washed with distilled water, then degreased with acetone, dried, and re-weighed. The corrosion rate (*v*) and the inhibitor efficiency (IE$_{WL}$) of ASP were calculated using Equations (1) and (2) [20], respectively. The surface coverage, θ = IE$_{WL}$/100.

$$v \text{ (mm/y)} = \frac{\Delta W \times 87600}{A \times \rho \times T} \tag{1}$$

$$IE_{WL}(\%) = \frac{weight\ loss(blank) - weight\ loss\ (inhibitor)}{weight\ loss\ (blank)} \times \frac{100}{1} \tag{2}$$

where ΔW is the weight loss after immersion, ρ is the density of the carbon steel (g cm^3), T is the immersion time, A is surface area of the coupons, and 87,600 is the conversion factor.

2.3. Electrochemical Measurements

The electrochemical experiments (electrochemical impedance spectroscopy (EIS)) and potentiodynamic polarization (PDP)) were performed using a Gamry Potentiostat/Galvanostat/ZRA Reference 600+ workstation at different temperatures (60 °C, 70 °C, 80 °C, and 90 °C). The capacity of the reaction cell was 200 mL and the three–electrode system consisted of Ag/AgCl (sat. 4.2 M KCl) as reference electrode, a platinum rod as the counter electrode, and the T95 carbon steel as working electrode. Before the EIS measurements, the working electrode was allowed to freely corrode at open circuit potential (OCP) for 1800 s in order to establish a steady-state condition required for EIS measurement. Thereafter, the electrochemical impedance spectroscopy measurement was performed under potentiostatic mode by applying an alternating–current signal at the frequency range of 100,000 Hz to 0.01 Hz utilizing an amplitude of 10 mV. After the EIS experiments, the T95 carbon steel electrode was scanned within the potential range of −250 to +250 mV with respect to the open circuit potential, at the rate of 1 mV/s. The analysis of the EIS and the PDP data was achieved via the Echem Analyst software. The inhibition efficiency was calculated for EIS using Equation (3) and for PDP using Equation (4) [21]:

$$\%\text{IE}_{\text{EIS}} = \frac{R_{ct\ (inhibited)} - R_{ct\ (blank)}}{R_{ct\ (inhibited)}} \times 100 \tag{3}$$

$$\%\text{IE}_{\text{PDP}} = \frac{i_{corr\ (blank)} - i_{corr\ (inhibited)}}{i_{corr\ (blank)}} \times 100 \tag{4}$$

2.4. Surface Characterization

The surfaces of the corroded T95 carbon steel surfaces at 60 °C and 90 °C after 4 h of immersion were observed in a JEOL JSM-6610 LV scanning electron microscope (SEM) that is coupled with an energy dispersive X-ray spectrophotometer (EDX) for elemental composition determination. The samples for the surface characterization experiments were prepared by immersing the pre-cleaned coupons for 4 h in 15 wt.% HCl solution without and with 2000 ppm ASP at 60 °C and 90 °C. Afterward, the samples were rinsed with distilled water, dried in warm air, and submitted for SEM, EDX, and 3D optical surface examinations. The 3D optical observation was performed using a 3D optical profilometer (Contour GT-K, Bruker Nano GmBH, Berlin, Germany).

3. Results

3.1. Weight-Loss Studies on the Performance of Aspartame as Inhibitor

Gravimetric measurements were undertaken to study the corrosion inhibition performance of ASP against T95 corrosion in 15 wt.% HCl solution at different temperatures, and the calculated corrosion parameters are listed in Table 1. It is shown in the table that the metal coupons, whether in uninhibited or inhibited acid solutions, lost weight. The known anodic oxidation and cathodic reduction corrosion reactions of carbon steel in acidic media proceed as $Fe \rightarrow Fe^{2+} + 2e^-$ and $2H^+ + 2e^- \rightarrow 2H_{ads} \rightarrow H_2 \uparrow$ [22]. These reactions, in addition to the high solubility of the corrosion products arising from the reactions, especially in the uninhibited acid solution, give rise to the metal samples losing weight [22]. Relative to the blank, the weight loss (WL) and corrosion rate (v) at all studied temperatures decreased in the inhibited systems. This indicates that ASP in the acid solution functioned as an inhibitor by protecting the metal surface from the corrosive attack. ASP, being an organic compound with O and N heteroatoms in its molecule (Figure 1), has the tendency to be adsorbed on the T95 surface and to obstruct active corrosion sites on the metal surface [23]. The influence of ASP on WL and v is seen to be concentration dependent. For instance, WL and v values decrease with increasing ASP concentration.

This could suggest that, in the acid solutions containing higher concentrations of ASP, more molecules of ASP were adsorbed on the metal surface and larger active sites were covered. The variations in the surface coverage (θ) and inhibition efficiency (IE$_{WL}$) according to ASP concentration seem to support this assertion. The observed increases in the values of θ and IE$_{WL}$ with increasing ASP concentrations imply a decrease in the electroactive area on the metal surface [24], meaning that more corrosion reaction sites were blocked upon the increase in the ASP concentration [24].

Table 1. Weigh loss (WL), corrosion rate (*v*), surface coverage (θ), and inhibition efficiency (IE) for T95 carbon steel corrosion in 15 wt.% HCl solution in the absence and presence of different concentrations of aspartame (ASP) at different temperatures from weight-loss measurements.

Conc. (ppm)	WL ± S.D (g)	(v ± S.D) × 10^{-3} (g cm^{-2} h^{-1})	θ	%IE$_{WL}$
		60 °C		
0	0.151 ± 0.004	4.199 ± 0.004	-	-
500	0.125 ± 0.011	3.471 ± 0.011	0.173	17
1000	0.104 ± 0.014	2.894 ± 0.014	0.311	31
1500	0.087 ± 0.001	2.413 ± 0.001	0.425	43
2000	0.076 ± 0.002	2.103 ± 0.002	0.499	50
		70 °C		
0	0.347 ± 0.020	9.639 ± 0.020	-	-
500	0.244 ± 0.014	6.779 ± 0.014	0.297	30
1000	0.192 ± 0.002	5.326 ± 0.002	0.447	45
1500	0.167 ± 0.011	4.628 ± 0.011	0.520	52
2000	0.147 ± 0.001	4.074 ± 0.001	0.577	58
		80 °C		
0	0.612 ± 0.003	17.007 ± 0.003	-	-
500	0.361 ± 0.001	10.036 ± 0.001	0.410	41
1000	0.290 ± 0.013	8.058 ± 0.013	0.526	53
1500	0.263 ± 0.003	7.315 ± 0.003	0.570	57
2000	0.227 ± 0.008	6.296 ± 0.008	0.630	63
		90 °C		
0	0.862 ± 0.048	23.935 ± 0.048	-	-
500	0.244 ± 0.001	6.767 ± 0.001	0.717	72
1000	0.190 ± 0.006	5.269 ± 0.006	0.780	78
1500	0.172 ± 0.006	4.781 ± 0.006	0.800	80
2000	0.123 ± 0.011	3.415 ± 0.011	0.857	86

It is also shown in Table 1 and Figure 2 that WL, *v*, θ, and IE$_{WL}$ increase with rises in the system temperature. The increase of WL and *v* with rises in temperature is as expected considering the fact that the rate of a chemical reaction is accelerated at higher temperatures [25]. Nevertheless, the increase in WL and *v* is at a greater magnitude in the 15 wt.% HCl solution without ASP than in the solution containing ASP, indicating the inhibiting effect of ASP. The increases in θ and IE$_{WL}$ with rises in temperature are characteristics of an organic inhibitor that is adsorbed via a chemisorption mechanism [26,27]. Chemisorption involves an exchange of electrons between specific surface sites and inhibitor molecules or the transfer of electrons from the inhibitor molecule to the vacant orbital of the absorbent, resulting in the formation of chemical bond(s). Chemisorption bonds are stronger and

more stable at high temperatures. Abdulazeez et al. [28] reported that a newly synthesized polyurea-based material (PUCorr-1) inhibited the corrosion of mild steel in a simulated acidic medium saturated with CO_2 and H_2S gases through the chemisorption mechanism. Other authors also reported corrosion inhibition via the chemisorption mechanism [29–31]. In the report, the inhibition efficiency of PUCorr-1 increased from 98.3% at 25 °C to 99.9% at 50 °C.
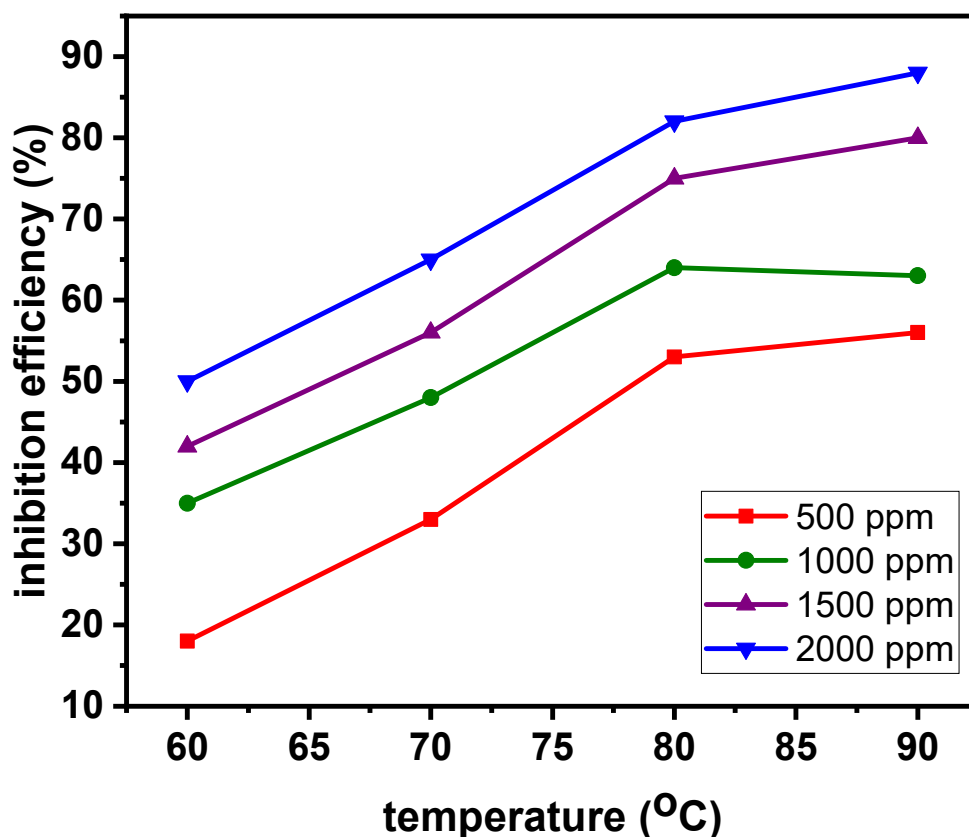

Figure 2. Variations in inhibition efficiency of ASP with temperature from weight-loss measurements.

It is worth pointing out the significant reduction of v by the 2000 ppm ASP from $23.935 \times 10^{-3} \pm 0.048 \text{ g cm}^{-2} \text{ h}^{-1}$ to $3.415 \times 10^{-3} \pm 0.011 \text{ g cm}^{-2} \text{ h}^{-1}$ and the IE_{WL} of 86% at 90 °C, which could imply stronger adsorption bonds and a dense and thick adsorption layer at this temperature. The solubility of ASP no doubt plays a remarkable role in the observed improved inhibition performance at higher temperatures. ASP solubility increased with increases in temperature [32]. It therefore means that, as the temperature of the solution was increased, more ASP dissolved and was available for adsorption and in extension inhibition.

3.2. Electrochemical Studies

3.2.1. OCP and EIS

It is a major requirement that system stability be achieved before electrochemical impedance spectroscopy (EIS) measurements are taken [33]. To satisfy this requirement, the T95 carbon steel working electrode was allowed to freely corrode in the 15 wt.% HCl solution under open circuit potential (OCP) for 1800 s. The variation in the OCP by immersion duration for the T95 steel immersed in 15% HCl solution without and with ASP at 60, 70, 80, and 90 °C is shown in Figure 3. It is obvious that, at least a pseudo-steady-state condition was achieved in all cases; hence, the EIS results presented herein can be relied upon. It should be mentioned that a completely steady-state condition is practically impossible since corrosion is dynamic in nature [34]. Worthy of noting also, as shown in

Figure 3, is the mixed-type behavior of the ASP. As can be seen in the graphs, at all studied temperatures, the extent of the displacement of the OCP by ASP relative to the blank is less than 85 mV vs. Ag/AgCl is needed for ASP classification as an anodic- or cathodic-type inhibitor [35,36]. ASP thus behaves as a mixed-type corrosion inhibitor.
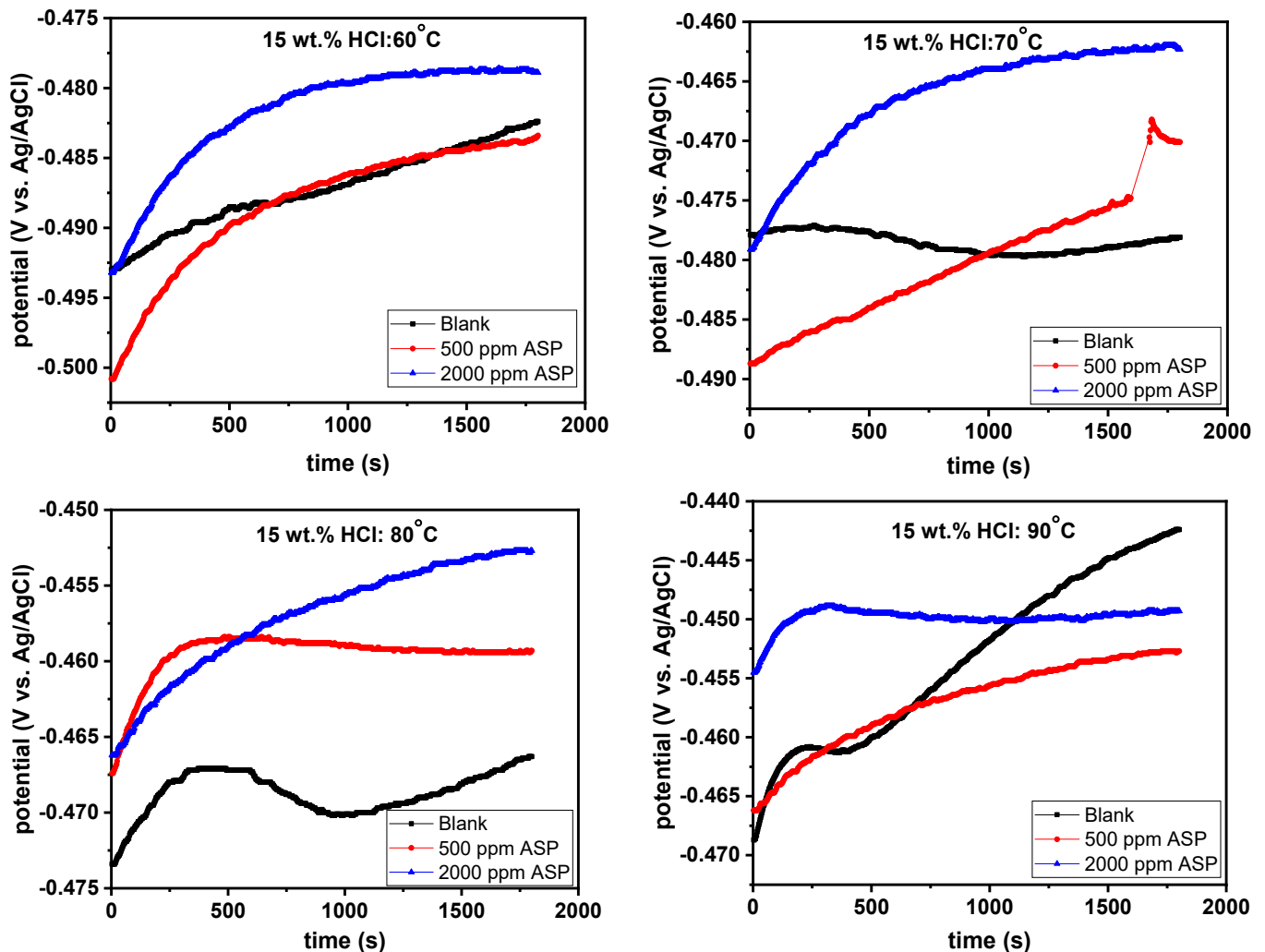

Figure 3. Variations in open circuit potential (OCP) by time for T95 carbon steel corrosion in 15 wt.% HCl solution without and with selected concentrations of aspartame at different temperatures.

At the steady OCP, the impedance characteristics of the T95 steel electrode in 15 wt.% HCl solution at the studied temperatures were collected. Figure 4 shows the Nyquist electrochemical plots for T95 carbon steel corrosion in 15 wt.% HCl solution without and with selected concentrations of ASP at different temperatures. The corresponding Bode representation is shown in Figure 5. The Nyquist diagrams, except that of the blank at 90 °C, exhibit an imperfect, single capacitive loop at the high-to-medium frequencies and an inductive loop at the low frequencies. The semi-circle at the high-to-medium frequencies implies that the corrosion of the T95 steel in the examined environment is governed by a charge transfer process [37,38]. The inductive loop is caused by the relaxation of the corrosion products or the adsorbed ASP molecules [39]. The imperfectness of the semi-circle is due to the micro-roughness and heterogeneity of the steel electrode [40,40]. At 90 °C, the Nyquist graph, in addition to the charge-controlled capacitive loop and the inductive loop, exhibits a poorly resolved semi-circle at the medium frequencies, and in the Bode representation (Figure 5), at the lower frequencies, log /Z/ seems to be independent of log f. These behaviors are typical of Warburg impedance and are common with a corrosion

system with diffusion contribution [41,42]. In such a system, reactants are transported from the bulk solution to the metal/solution interface or soluble products are transported from the metal/solution interface to the bulk solution [41,42]. Compared to the blank, it can be seen that, at all the studied temperatures, the size of the capacitive loop of the inhibited graphs is larger, with the 2000 ppm ASP-inhibited graphs being the largest. This is reflective of the inhibitive effect of ASP at 2000 ppm exhibiting a higher protective effect than the ASP at 500 ppm. The effect of concentration on the inhibitive performance of ASP is also seen in the Bode representation (Figure 5). In Figure 5, the impedance modulus and the phase angle tilt toward nobler values with increasing concentrations. The implication is that the rate of the charge transfer process was slowed down in the ASP-inhibited systems due to the adsorption of the ASP molecules onto the T95 surface and the covering of the active sites [43,44]. The anti-corrosion performance of ASP at higher concentrations is superior to that at lower concentrations.
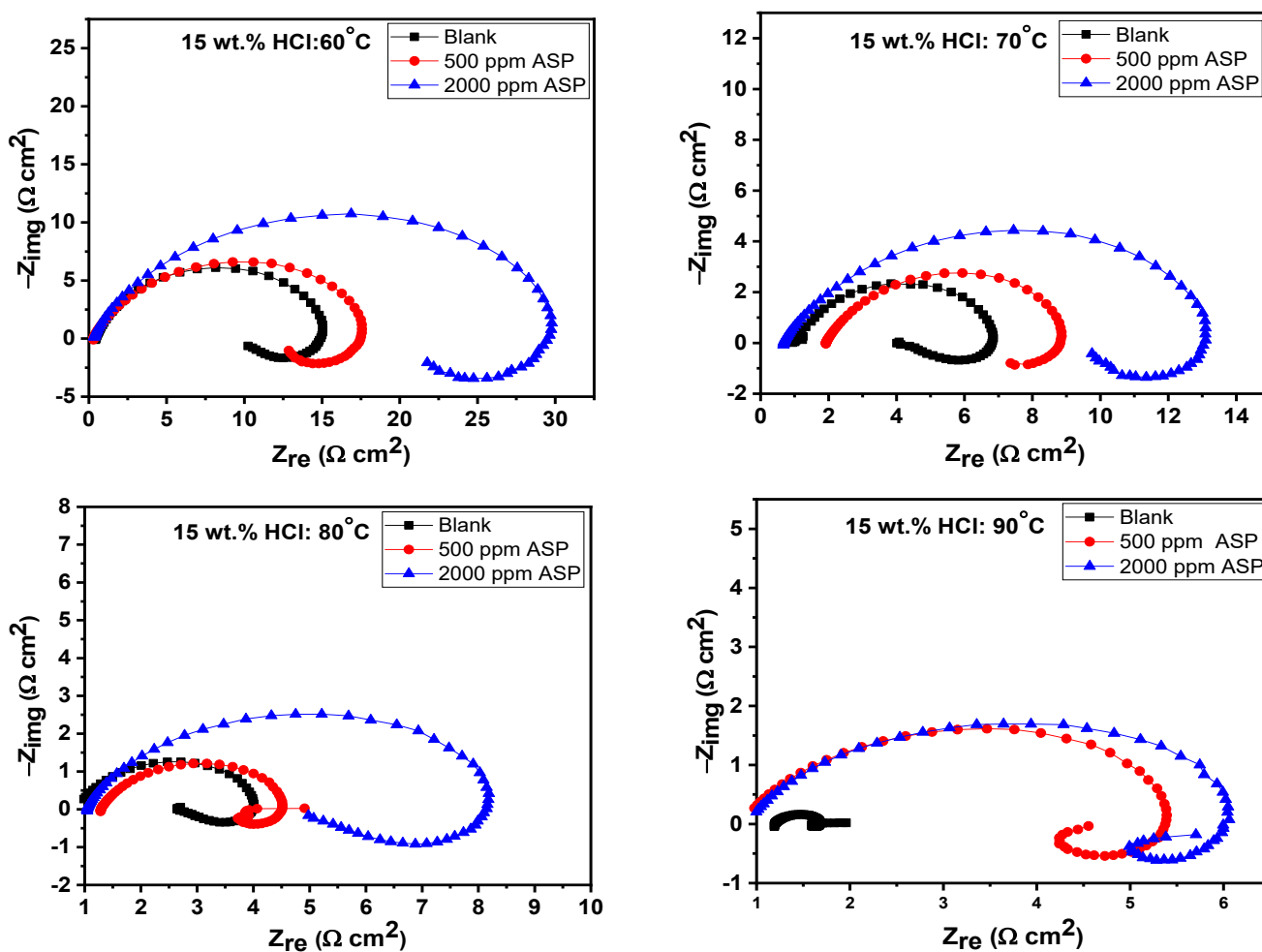

Figure 4. Nyquist electrochemical plots for T95 carbon steel corrosion in 15 wt.% HCl solution without and with selected concentrations of aspartame at different temperatures.

Figure 5. Bode electrochemical plots for T95 carbon steel corrosion in 15 wt.% HCl solution without and with selected concentrations of aspartame at different temperatures.
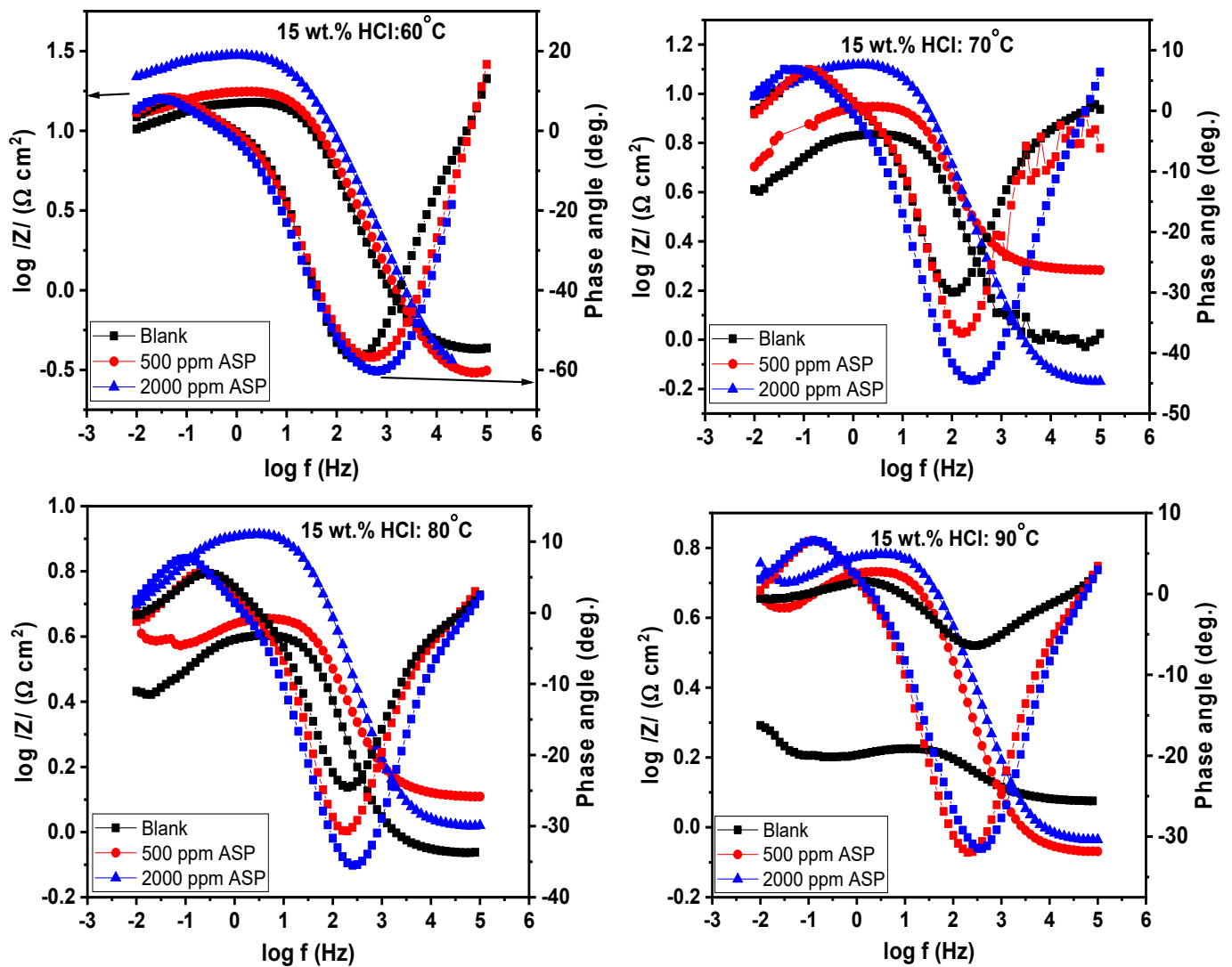
The impedance data were fitted using the equivalent circuits (ECs) shown in Figure 6. The various phenomena observed in Figures 4 and 5 were taken into consideration in the selection of the ECs. The EC in Figure 6a was used for the analysis of all the EIS data except the data for the blank at 90 °C. The EC consists of the following elements: R_s (solution resistance), C (corrosion/adsorbed products capacitance), R_f (film resistance), R_{ct} (charge transfer resistance), and L (inductor). Because of the diffusion phenomenon observed in Figures 4 and 5 at 90 °C, the EC in Figure 6b was used for the analysis of the EIS data for the blank at 90 °C. It has the element, W (Warburg impedance), in addition to the other elements in Figure 6a. The suitability of the selected ECs is reflected in the low fitting error and the low chi square values listed in Table 2. All the values obtained from the fitting are given in Table 2. The inhibition efficiency (IE_{EIS}) values, also given in the table, were calculated using Equation (3). R_p is the total resistance, that is $R_{ct} + R_f$. It is clear from the table that R_p of the T95 steel increased in the ASP-inhibited systems relative to the uninhibited, indicating that the presence of the ASP in the HCl solution boosted the corrosion resistance property of the metal. The best effect is observed for the 2000 ppm–inhibited systems. At 60 °C, the presence of 2000 ppm ASP in the acid solution caused a 47% increase in R_p, from 13.52 ± 0.29 Ω cm^2 to 25.31 ± 0.98 Ω cm^2, meaning that the metal surface was more protected by 47%. It is also seen that the corrosion inhibition performance of ASP

improves with increase in temperature and is in excellent agreement with the results from the weight-loss experiments (Table 1). For 2000 ppm ASP, the IE_{EIS} increased from 47% at 60 °C to 51% at 70 °C. With further increase in the system temperature to 80 °C and 90 °C, IE_{EIS} increased to 62% and 85%, respectively. These results indicate that ASP is a promising corrosion inhibitor for high-temperature acidizing applications. ASP could be employed as an active compound for inhibitor formulation intended for acidizing applications. It is worth mentioning that the value of *n* obtained for the blank at 90 °C is 0.51, which signifies Warburg impedance [41,42] and thus confirms the presence of diffusion at 90 °C [41,42].
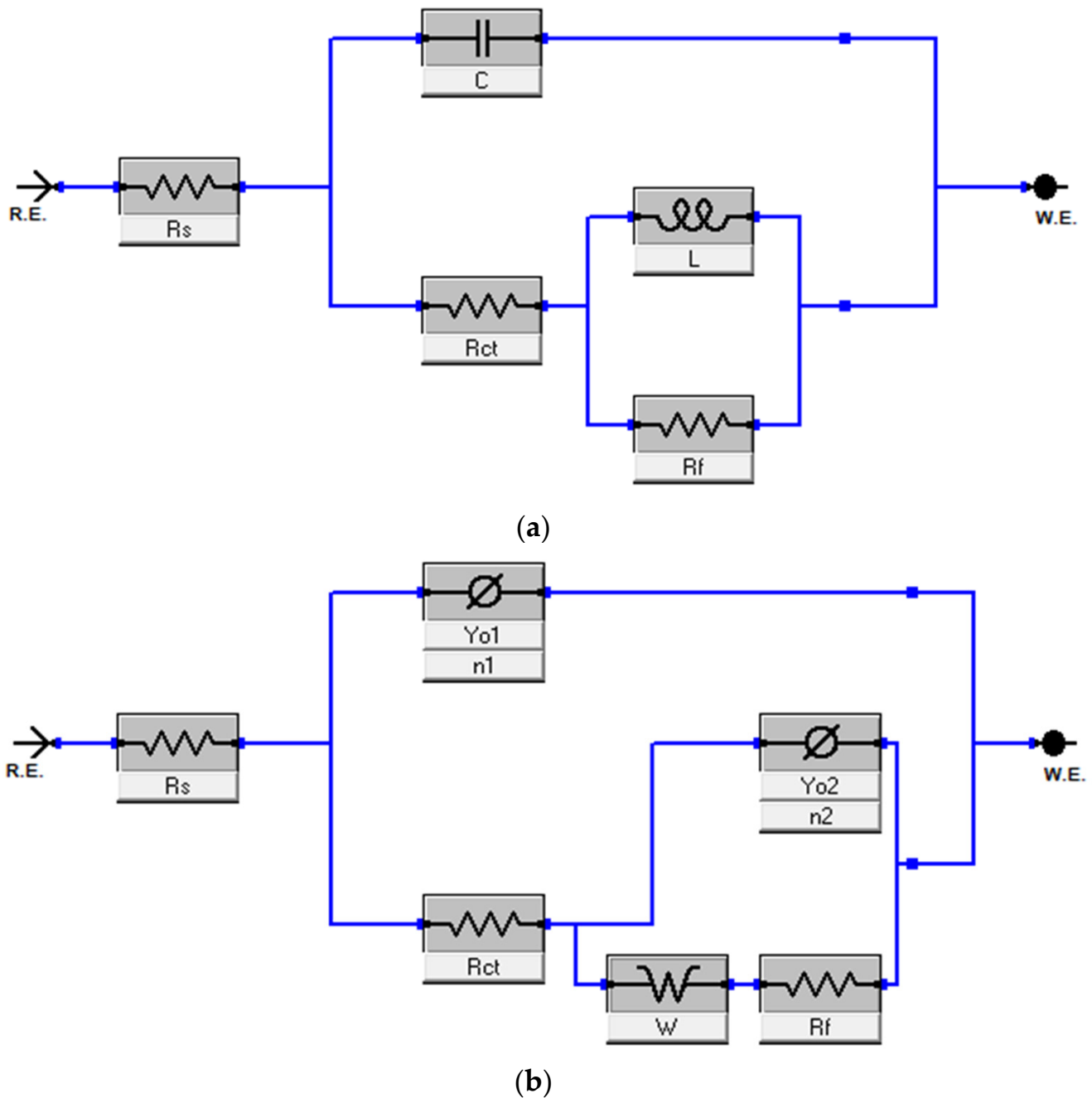

(**a**)

(**b**)

Figure 6. Equivalent circuit used in the analysis of (**a**) all the electrochemical impedance data except the data for blank at 90 °C, in which (**b**) was used.

Table 2. EIS parameters derived for T95 carbon steel during corrosion in 15 wt.% HCl at different temperatures without and with 500 ppm and 2000 ppm aspartame.

Conc. (ppm)	$R_s \pm Er$ ($\Omega\ cm^2$)	$R_{ct} \pm Er$ ($\Omega\ cm^2$)	$R_f \pm Er$ ($\Omega\ cm^2$)	$L \pm Er$ (H)	$(C \pm Er) \times 10^{-4}$ (F)	x^2 $\times 10^{-3}$	$R_p \pm Er$ ($\Omega\ cm^2$)	%IE$_{EIS}$
				60 °C				
0	0.48 ± 0.003	9.98 ± 0.14	3.54 ± 0.15	10.50 ± 1.14	2.43 ± 0.00	21.9	13.52 ± 0.29	-
500	0.34 ± 0.003	11.76 ± 0.20	3.56 ± 0.20	15.60 ± 2.22	1.80 ± 0.00	44.2	15.32 ± 0.40	12
2000	0.42 ± 0.006	19.38 ± 0.50	5.93 ± 0.48	47.92 ± 9.11	1.31 ± 0.00	53.5	25.31 ± 0.98	47
				70 °C				
0	1.07 ± 0.006	3.38 ± 0.05	1.98 ± 0.06	2.68 ± 0.20	3.95 ± 0.00	9.63	5.36 ± 0.11	-
500	2.05 ± 0.012	5.57 ± 0.28	1.82 ± 0.26	1.98 ± 0.64	4.05 ± 0.00	5.95	7.39 ± 0.54	27
2000	0.77 ± 0.005	8.73 ± 0.14	2.14 ± 0.15	8.23 ± 1.42	2.38 ± 0.00	34.0	10.87 ± 0.29	51
				80 °C				
0	0.92 ± 0.006	1.89 ± 0.03	0.50 ± 0.03	0.85 ± 0.07	5.49 ± 0.00	5.89	2.39 ± 0.06	-
500	1.37 ± 0.008	2.46 ± 0.03	1.52 ± 0.04	0.23 ± 0.05	4.37 ± 0.00	5.16	3.98 ± 0.07	40
2000	1.14 ± 0.007	4.17 ± 0.07	2.13 ± 0.07	4.16 ± 0.36	2.53 ± 0.00	15.1	6.30 ± 0.14	62
				90 °C				
0	1.20 ± 0.012	0.44 ± 0.02	0.25 ± 0.17	-	-	0.92	0.69 ± 0.19	-
500	0.96 ± 0.006	3.26 ± 0.04	0.80 ± 0.05	1.09 ± 0.18	4.33 ± 0.00	12.9	4.06 ± 0.09	83
2000	1.02 ± 0.007	3.92 ± 0.06	0.61 ± 0.06	0.96 ± 0.24	2.66 ± 0.00	16.4	4.53 ± 0.12	85

3.2.2. PDP

The potentiodynamic polarization technique was used to investigate the cathodic and anodic corrosion kinetics of T95 steel at 60–90 °C in 15% HCl in the presence and absence of ASP. The polarization curves plotted for the studied systems are presented in Figure 7. In the comparison of the polarization curves for the blank to those of the ASP-inhibited treatments, a shift in both the anodic and cathodic curves towards the lower current zone is observed. Additionally, the displacement of the corrosion potential (E_{corr}) by the inhibitor is insignificant. These observations indicate that ASP acted as an inhibitor for T95 steel corrosion in the studied acid solution at all temperatures and that the inhibition was due to the ability of ASP to interrupt both the anodic oxidation of T95 steel and the cathodic reduction of adsorbed hydrogen to hydrogen gas [34,45]. In other words, ASP acted as a mixed-type corrosion inhibitor [34,45], which is in agreement with the OCP results (Figure 3).

The anodic and cathodic branches show Tafel-like regions; that is, the linear portions signify majorly activation-controlled corrosion kinetics [36,46]. These linear portions were extrapolated to obtain the polarization parameters, namely corrosion potential (E_{corr}), corrosion current density (i_{corr}), anodic Tafel slope (β_a), and cathodic Tafel slope (β_c), the values for which are given in Table 3. The corrosion rate (v) values were calculated using Equation (5) [47] and the inhibition efficiency (IE$_{PDP}$) values were calculated using Equation (4). From Table 3, the presence of ASP in the 15 wt.% HCl solution is seen to significantly diminish the corrosion current, particularly at 90 °C. For instance, at 90 °C, in the presence of 2000 ppm ASP, the i_{corr} value decreased from 201.00 mA cm^{-2} to 25.97 mA cm^{-2}. The low current density in the inhibited systems resulted in a low corrosion rate. The presence of 2000 ppm ASP reduced the v from 2326.686 mm/yr to 300.617 mm/yr, and this correspond to inhibition efficiency of 87%. Again, according to this technique, ASP is a highly promising corrosion inhibitor for high-temperature acidizing processes. A further inspection of Table 3 reveals that the changes in the E_{corr}, β_a, and β_c values of the inhibited systems and those of the uninhibited system are minimal.

For instance, $E_{\text{corr(inhibited)}} - E_{\text{corr(unhibited)}} =< 15$ mV vs. Ag/AgCl. This confirms the mixed-type behavior [34,45] of ASP earlier proposed.

$$v \; (\text{mm/y}) = 3.27 \times i_{\text{corr}} \times \frac{e}{\rho} \tag{5}$$

where 3.27 is a proportionality constant, e and ρ are the equivalent weight and density of steel, respectively, and i_{corr} is in mA cm^{-2}.
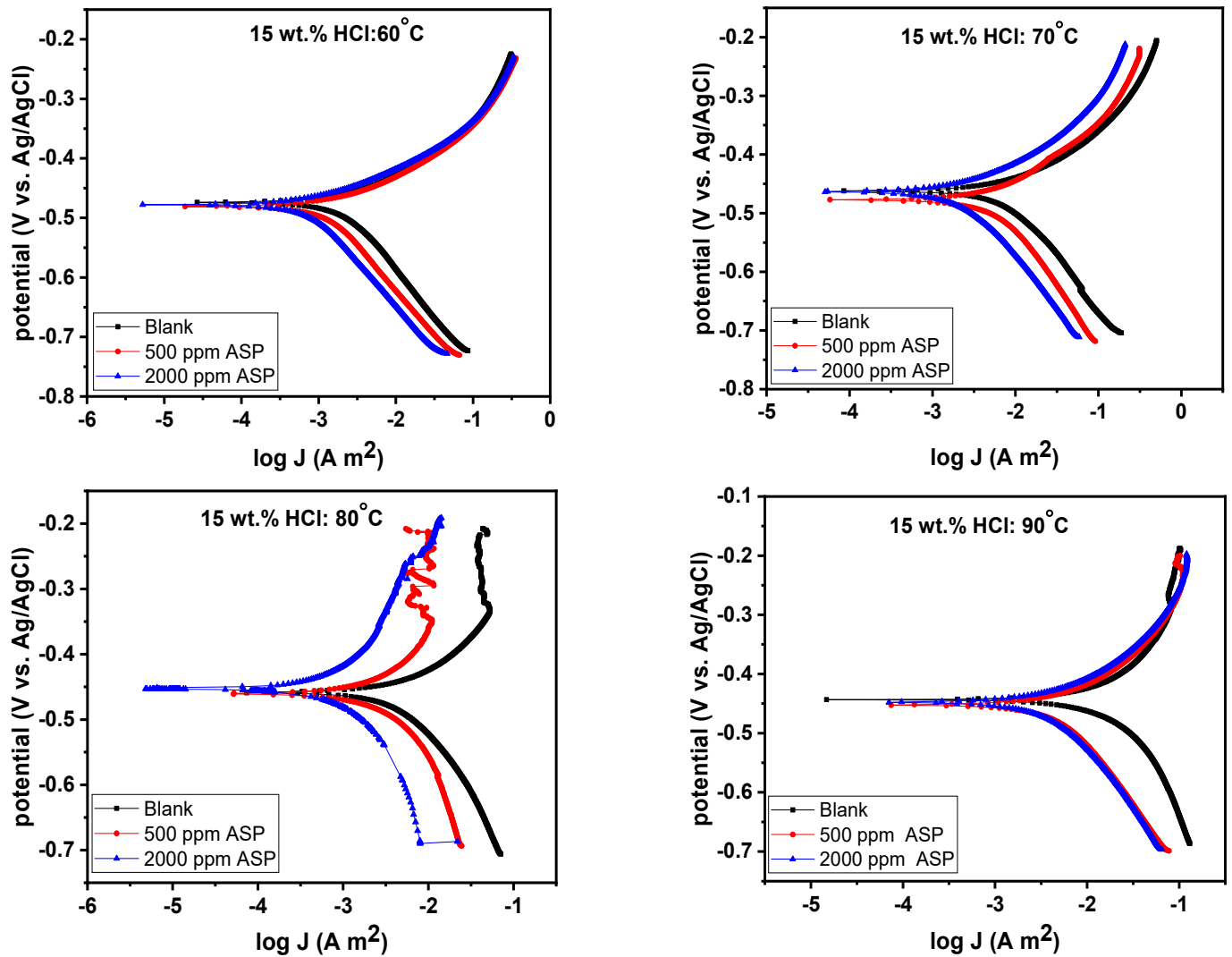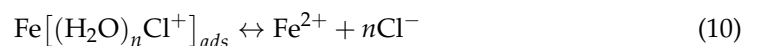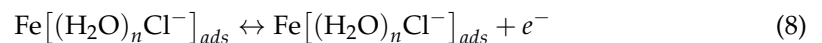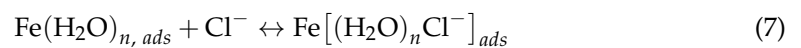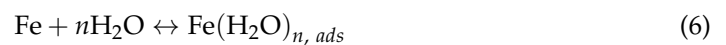

Figure 7. Potentiodynamic polarization graphs for T95 carbon steel corrosion in 15 wt.% HCl solution without and with selected concentrations of aspartame at different temperatures.

Table 3. Potentiodynamic polarization parameters derived for T95 carbon steel corrosion in 15 wt.% HCl solution without and with selected concentrations of aspartame at different temperatures.
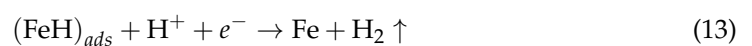
Conc. (ppm)	$-E_{corr}$ (mV vs. Ag/AgCl)	i_{corr} (mA cm^{-2})	β_a (V dec^{-1})	β_c (V dec^{-1})	v (mm/y)	IE$_{PDP}$ (%)
			60 °C			
0	474.0	2.24	62.30	173.40	25.929	-
500	481.0	1.91	51.20	162.70	22.109	15
2000	478.0	1.16	49.90	151.90	13.428	48
			70 °C			
0	477.0	11.7	135.90	531.20	135.434	-
500	462.0	8.51	84.40	189.40	98.508	27
2000	463.0	5.27	67.20	162.80	61.003	55
			80 °C			
0	460.0	62.50	2.29	3.37	723.472	-
500	453.0	34.96	0.08	1.87	404.681	44
2000	459.0	22.34	0.09	0.20	258.598	64
			90 °C			
0	443.0	201.00	1.54	2.09	2326.686	-
500	452.0	29.86	0.11	0.27	345.646	85
2000	448.0	25.97	0.10	0.21	300.617	87

3.3. Mechanism of Inhibition by Aspartame

The acceptable corrosion inhibition mechanism by organic inhibitors is the adsorption mechanism, whereby an organic molecule substitutes an adsorbed water molecule on a metal surface to form a protective film that decreases the rate at which corrosive species attack the surface [48,49]. It has already been established that the surface of carbon steel is positively charged in a highly concentrated HCl medium [36,50,51]. Additionally, chloride ions (Cl$^-$) are believed to be preferentially adsorbed on the positively charged steel surface [36,50,51]. Accordingly, the anodic oxidation reactions are as shown in Equations (6)–(10) [52] and the overall anodic oxidation of the T95 carbon steel in 15 wt.% HCl solution is illustrated in Figure 8a.

$$\text{Fe} + n\text{H}_2\text{O} \leftrightarrow \text{Fe}(\text{H}_2\text{O})_{n,\,ads} \tag{6}$$

$$\text{Fe}(\text{H}_2\text{O})_{n,\,ads} + \text{Cl}^- \leftrightarrow \text{Fe}\left[(\text{H}_2\text{O})_n\text{Cl}^-\right]_{ads} \tag{7}$$

$$\text{Fe}\left[(\text{H}_2\text{O})_n\text{Cl}^-\right]_{ads} \leftrightarrow \text{Fe}\left[(\text{H}_2\text{O})_n\text{Cl}^-\right]_{ads} + e^- \tag{8}$$

$$\text{Fe}\left[(\text{H}_2\text{O})_n\text{Cl}^-\right]_{ads} \rightarrow \text{Fe}\left[(\text{H}_2\text{O})_n\text{Cl}^+\right]_{ads} + e^- \tag{9}$$

$$\text{Fe}\left[(\text{H}_2\text{O})_n\text{Cl}^+\right]_{ads} \leftrightarrow \text{Fe}^{2+} + n\text{Cl}^- \tag{10}$$

The corresponding cathodic reduction reactions are given in Equations (11)–(13) [52] and illustrated in Figure 8b.

$$\text{Fe} + \text{H}^+ \leftrightarrow \left(\text{FeH}^+\right)_{ads} \tag{11}$$

$$\left(\text{FeH}^+\right)_{ads} + e^- \rightarrow \left(\text{FeH}\right)_{ads} \tag{12}$$

$$\left(\text{FeH}\right)_{ads} + \text{H}^+ + e^- \rightarrow \text{Fe} + \text{H}_2 \uparrow \tag{13}$$

In the HCl solution containing ASP, our potentiodynamic polarization results (Figure 5 and Table 3) reveal that both the anodic oxidation and the cathodic reduction reactions

were interrupted. Obviously, in the 15 wt.% HCl solution, ASP is protonated through the $-NH_2$ functional group (see Figure 1) such that it exists in cationic form (ASP^+). The ASP^+ is electrostatically attracted to the charged T95 steel surface [36,50,51], and thus, the anodic oxidation reaction in Equation (8) is interrupted, as shown in Equation (14) and illustrated in Figure 8c.

$$Fe\left[(H_2O)_n Cl^-\right]_{ads} + ASP^+ \rightarrow Fe\left[(H_2O)_n Cl^- ASP^+\right]_{ads} \tag{14}$$
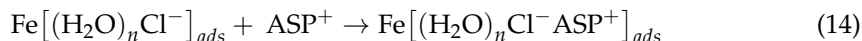
Moreover, our results (Tables 1–3) disclose that ASP molecules were chemically adsorbed on the steel surface; that is, chemical bonds were formed between ASP and the steel surface. ASP, as can be seen in Figure 1, still has other O, N, and even the benzene ring, which are rich in electron pairs. Therefore, it is possible that, upon attraction to the steel surface via coulombic electrostatic attraction, electron pairs were donated to the low energy 3d-orbital of Fe. Such behavior was previously reported for *N*-(2-(2-tridecyl-4,5-dihydro-1H-imidazol-1-yl)ethyl)tetradecanamide in 15 wt.% HCl solution [36].

At the cathodic region, ASP^+ and H^+ can undergo competitive adsorption [52] such that the adsorbed ASP inhibits the cathodic reduction reactions according to Equations (15) and (16) as well as the illustration in Figure 8d.
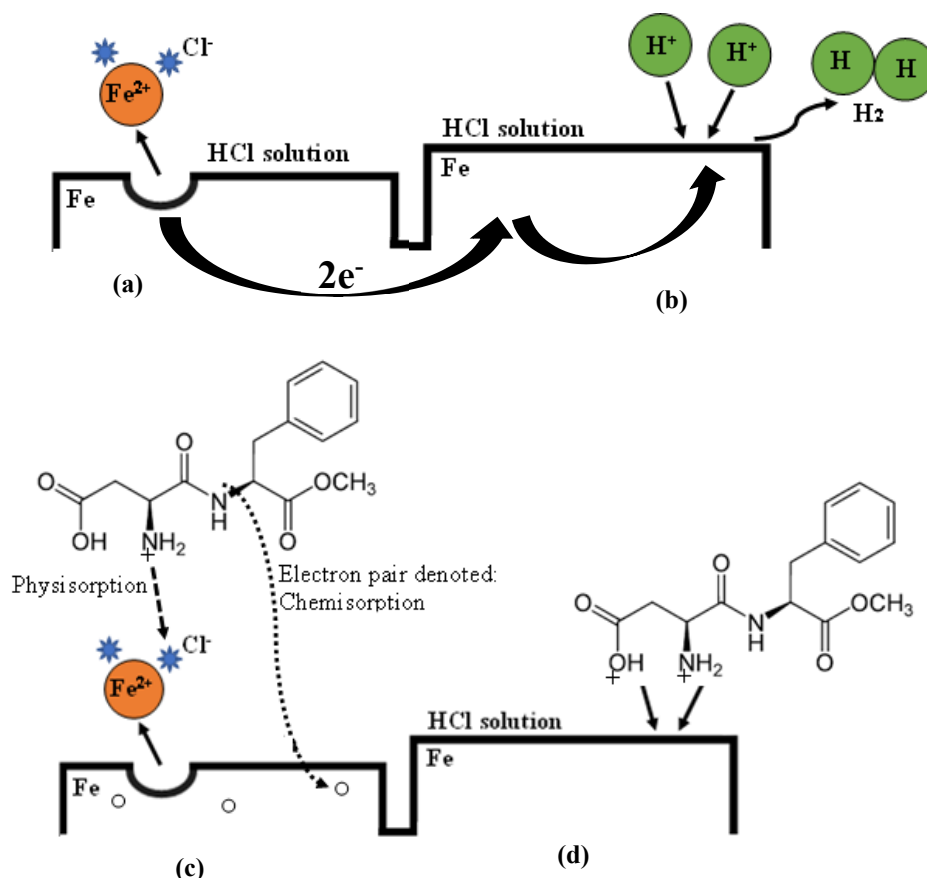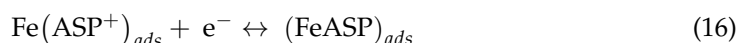
$$Fe + ASP^+ \leftrightarrow Fe\left(ASP^+\right)_{ads} \tag{15}$$

$$Fe\left(ASP^+\right)_{ads} + e^- \leftrightarrow (FeASP)_{ads} \tag{16}$$

Figure 8. An illustration of the corrosion of T95 carbon steel in 15 wt.% HCl solution and inhibition by aspartame. (**a**) Anodic reaction: $Fe \rightarrow Fe^{2+} + nCl^- + 2e^-$, (**b**) Cathodic reaction: $H^+ + 2e^- \rightarrow H_2$, (**c**) Adsorption of Aspartame on the anodic region: $Fe\left[(H_2O)_n Cl^-\right]_{ads} + ASP^+ \rightarrow Fe\left[(H_2O)_n Cl^- ASP^+\right]_{ads}$, and (**d**) Adsorption of Aspartame on the cathodic region: $Fe\left(ASP^+\right)_{ads} + e^- \leftrightarrow (FeASP)_{ads}$.

3.4. Surface Analysis

3.4.1. SEM and EDX

The surface morphology of the abraded T95 steel, the steel specimens immersed in 15 wt.% HCl solution without ASP at 60 °C and 90 °C, and the steel specimens immersed in 15 wt.% HCl solution containing 2000 ppm of ASP at 60 °C and 90 °C after 4 h of immersion are shown in Figure 9. The elemental composition of the surfaces at 90 °C, as obtained by energy dispersive X-ray spectrophotometry (EDX), are given in Figure 10. As can be seen in Figure 9a, the steel surface after mechanical abrasion was smooth, and Fe (85.9%), Cr (8.6%), C (3.6%), Mo (1.1%), Si (0.4%), Mn (0.3%), and Ni (0.1%) were detected (Figure 10a), which agrees with the composition of the T95 steel listed in Section 2.1. The steel surface was significantly impacted by corrosion in the absence of the inhibitor, resulting in a rough surface with heaps of porous corrosion products (Figure 9b,c). The EDX results in Figure 10b disclose that the corrosion product is enriched with Cl (20.5%), O (11.0%) and C (10.5%). This indicates that the corrosion products on the steel surface are mixtures of carbonates, chlorides, and oxides, in conformity with previous reports [36]. Compared to the surfaces in Figure 9b,c, the ASP-inhibited surfaces in Figure 9d,e exhibit smoother morphology and the surface deposits are more compact. In the EDX spectrum in Figure 10c, there is a noticeable decrease in the percentage of Cl (16.3%) and O (8.3%), meaning that the formation of the corrosion products was abated. The detection of N (1.0%) and the increase in C (12.7%) content provide experimental evidence of the adsorption of ASP on the steel surface. The adsorbed ASP film was thus responsible for the inhibition of the steel corrosion, in agreement with the results from other applied techniques.

3.4.2. Optical Profilometer

The surface of the corroded T95 steel was further studied using an optical profilometer. Our interest in this study was on the roughness characteristics of the corroded surface in comparison with the roughness properties of the abraded surface. Figure 11 shows the surface profilometer images taken for the T95 steel specimen after mechanical abrasion and after exposure to a 15 wt.% HCl solutions devoid of and containing 2000 ppm ASP for 4 h at 60 and 90 °C. The values of the roughness parameters derived for the surfaces are presented in Table 4. The parameters include R_a, which is the average value of profile deviation from the mean line; R_t, the total height which is used to describe the largest peak to valley height; and the mean width of the primary profile element (R_{RMS}) [36,43]. The smooth surface in Figure 11a has R_a, R_t, and R_{RMS} values of 0.154 μm, 2.119 μm, and 0.186 μm, respectively. It is very visible that the metal surface was severely damaged by corrosion at the studied temperatures. The surface became very rough due to corrosion (Figure 11b,c). The R_a, R_t, and R_{RMS} values increased to 2.269 μm, 39.708 μm, and 2.933 μm, respectively, at 60 °C and to 4.350 μm, 93.215 μm, and 5.679 μm, respectively, at 90 °C. However, the steel surface was protected in the acid solution containing ASP, such that the surface roughness greatly decreased (Figure 11d,e). As can be seen in Table 4, the R_a, R_t, and R_{RMS} values are reduced by 41%, 73%, and 40%, respectively, at 60 °C and by 86%, 66%, and 89%, respectively, at 90 °C. This shows the excellent corrosion-protective ability of ASP. It can again be seen that ASP is very effective at 90 °C.
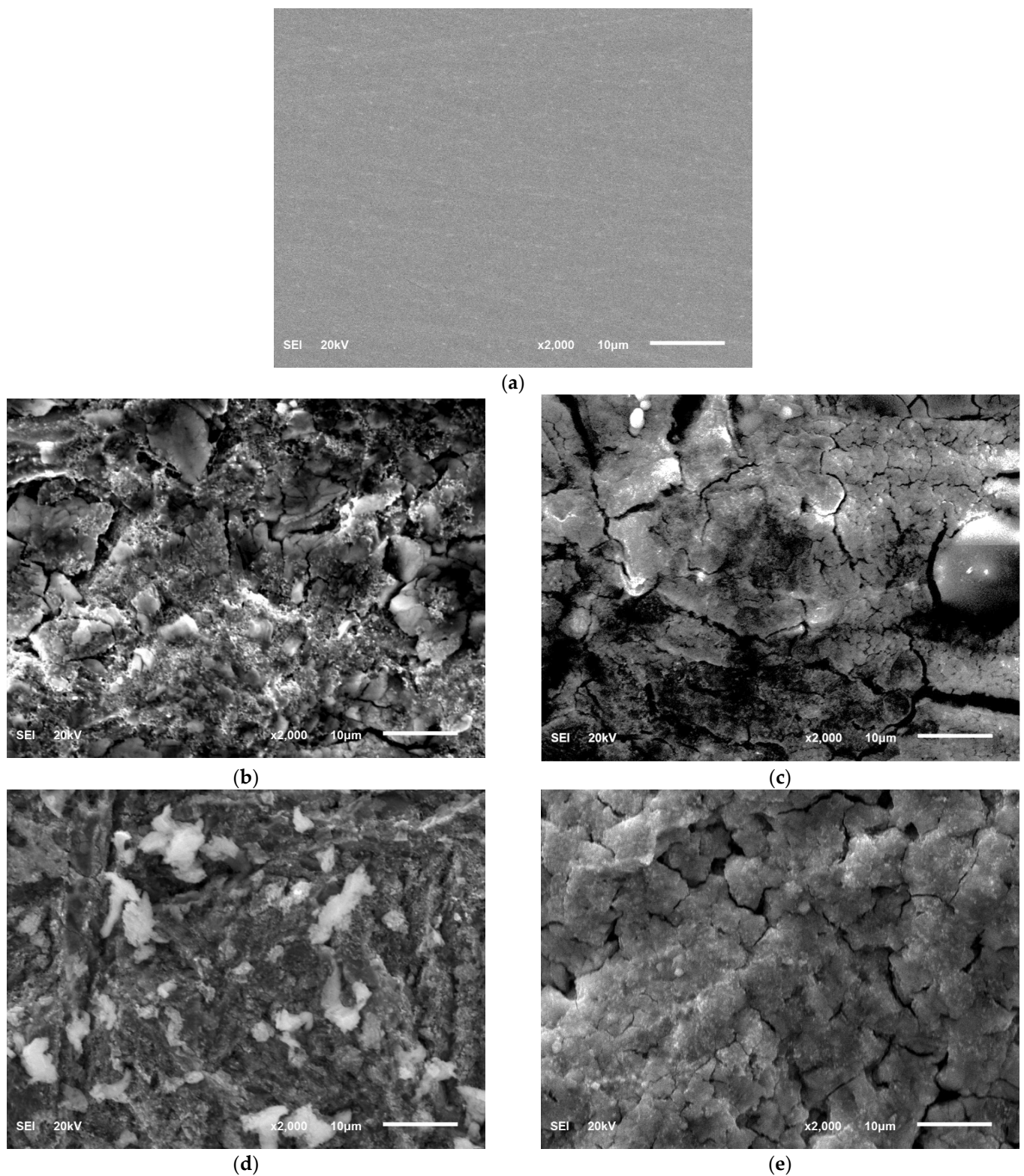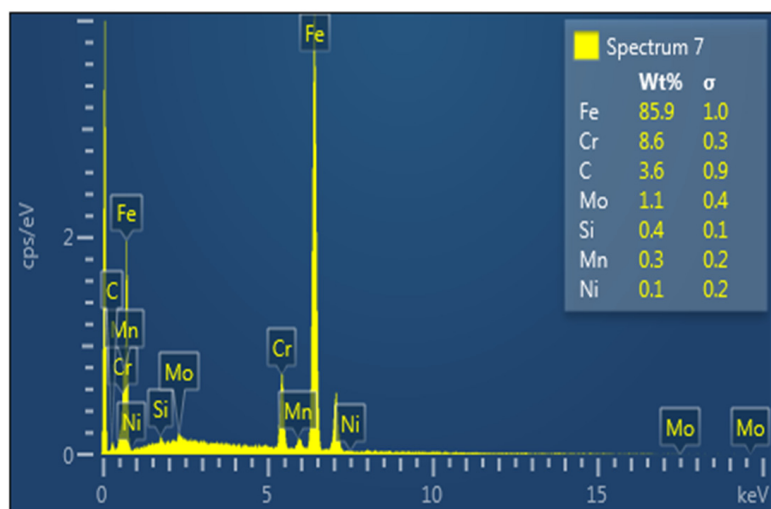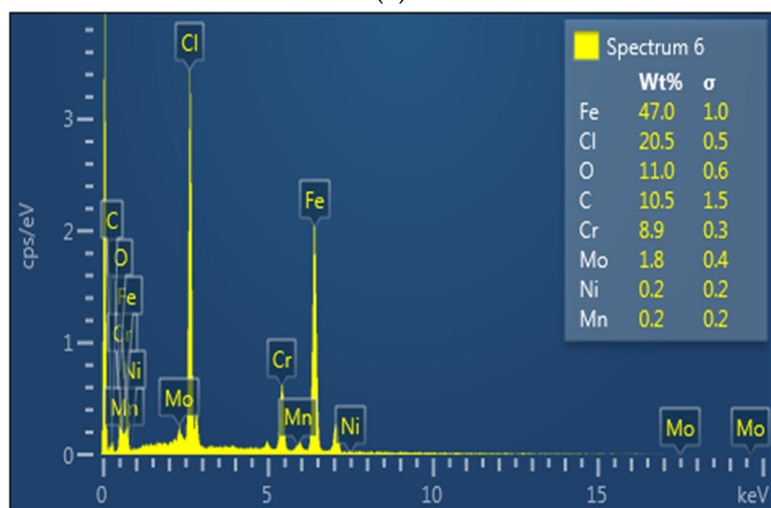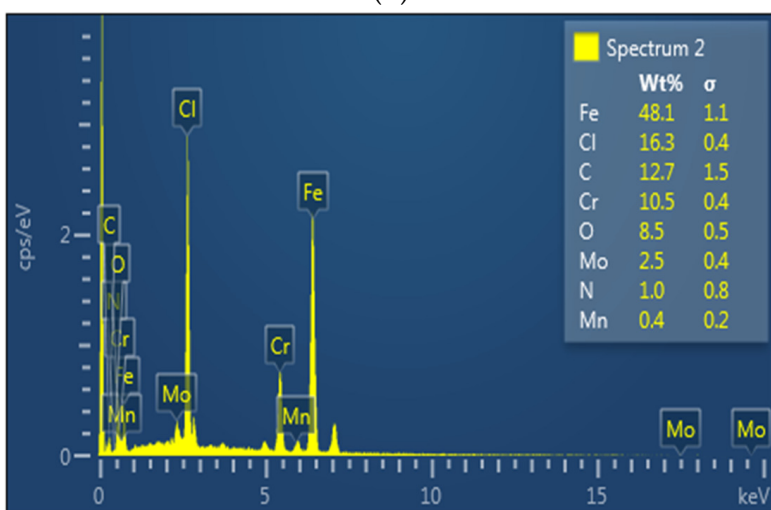
(**a**)

(**b**)

(**c**)

(**d**)

(**e**)

Figure 9. SEM micrographs of (**a**) the abraded T95 steel, the steel specimens immersed in 15 wt.% HCl solution without the inhibitor at (**b**) 60 °C and (**c**) 90 °C, and the steel specimens immersed in 15 wt.% HCl solution containing 2000 ppm of aspartame at (**d**) 60 °C and (**e**) 90 °C after 4 h of immersion.

Figure 10. EDX spectra of (**a**) the abraded T95 steel, (**b**) the steel specimens immersed in 15 wt.% HCl solution without the inhibitor, and (**c**) the steel specimens immersed in 15 wt.% HCl solution containing 2000 ppm of inhibitor at 90 °C after 4 h of immersion.
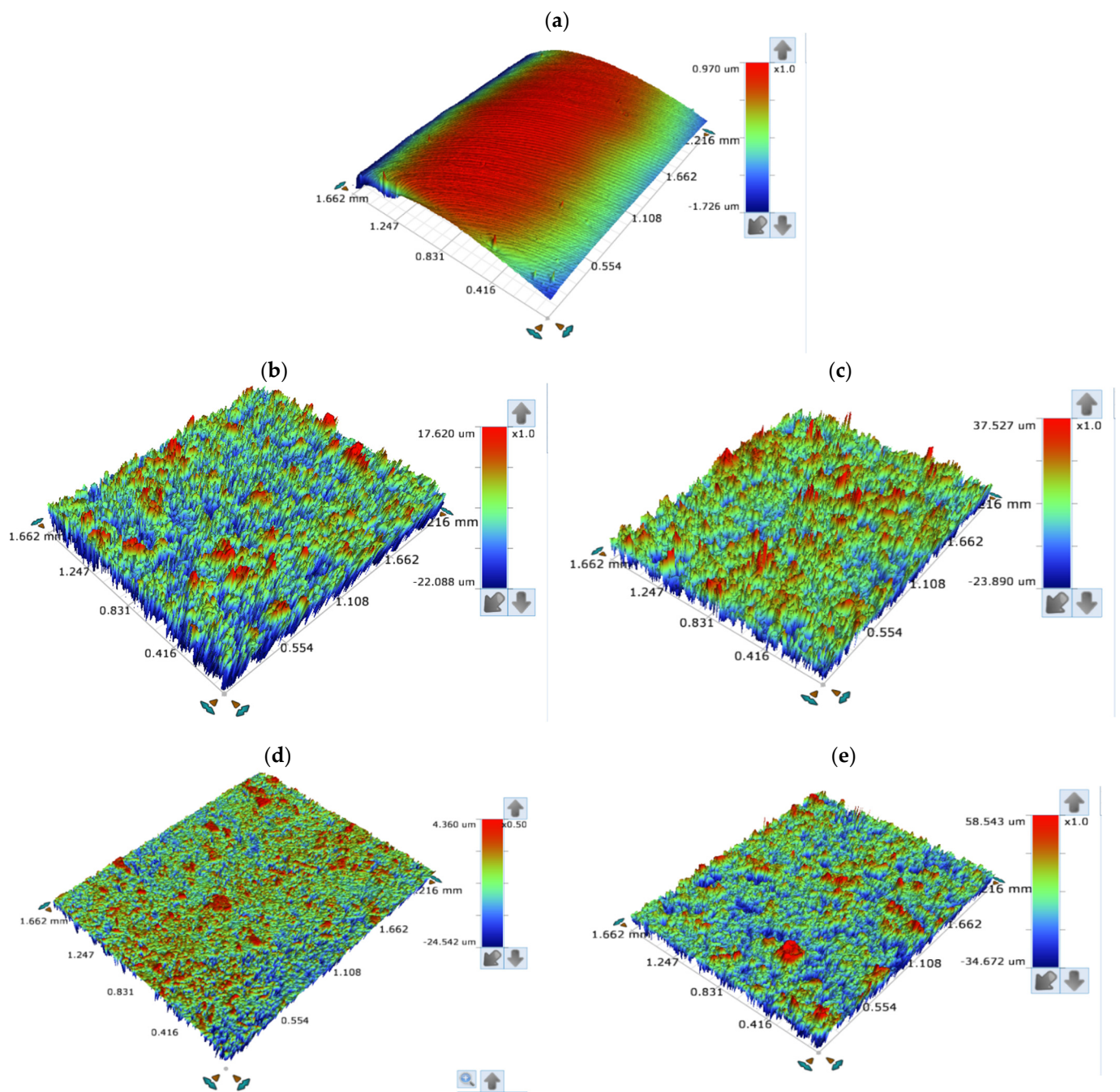
Figure 11. Surface profilometer images of (**a**) the abraded T95 steel, the steel specimens immersed in 15 wt.% HCl solution without the inhibitor at (**b**) 60 °C and (**c**) 90 °C, and the steel specimens immersed in 15 wt.% HCl solution containing 2000 ppm of aspartame at (**d**) 60 °C and (**e**) 90 °C after 4 h of immersion.

Table 4. Surface parameters derived from profilometer surface analysis of the corroded T95 steel immersed in 15% HCl without and with additives at 90 °C after 4 h immersion.

Systems/Concentration	Surface Roughness					
	R_a (μm)	R_{RMS} (μm)	R_t (μm)	R_a (μm)	R_{RMS} (μm)	R_t (μm)
	60 °C			90 °C		
Abraded T95 steel	0.154	0.186	2.119	0.154	0.186	2.119
Blank	2.269	2.933	39.708	4.350	5.679	93.215
2000 ppm Aspartame	0.925	1.170	28.902	3.736	5.029	61.417
% Reduction	41	40	73	86	89	66

4. Summary and Conclusions

The corrosion inhibition ability of aspartame (ASP) for T95 carbon steel in 15 wt.% HCl at 60–90 °C was studied using the weight-loss, electrochemical impedance spectroscopy, potentiodynamic polarization, scanning electron microscope, energy dispersive X-ray, and optical profilometric techniques. It was found, from all the applied techniques, that ASP is a promising corrosion inhibitor for acidizing processes. The inhibition efficiency of ASP increased with increases in temperature, reaching 86% with 2000 ppm ASP at 90 °C. ASP acts as a mixed-type corrosion inhibitor, interfering in both the anodic and cathodic reactions. The optical profilometry results show that the R_a, R_t, and R_{RMS} values were reduced by 41%, 73%, and 40%, respectively, at 60 °C and by 86%, 66%, and 89%, respectively, at 90 °C in the presence of ASP. This shows the excellent corrosion-protective ability of ASP. All the results are in good agreement and the EDX results provide evidence of ASP adsorption on the steel surface. ASP is recommended as an active compound for inhibitor formulations intended for acidizing applications at high temperatures.

Author Contributions: Conceptualization, M.M.S. and I.E.U.; methodology, M.M.S., I.E.U. and S.A.U.; validation, M.M.S. and S.A.U.; formal analysis, M.M.S., R.T.L., I.E.U. and S.A.U.; investigation, M.M.S. and I.E.U.; resources, M.M.S., R.T.L., I.E.U. and S.A.U.; data curation, M.M.S., S.A.U. and I.E.U.; writing—original draft preparation M.M.S. and I.E.U.; writing—review and editing, M.M.S., R.T.L., I.E.U. and S.A.U.; visualization, M.M.S.; supervision, M.M.S. and S.A.U.; project administration, M.M.S.; funding acquisition M.M.S. and I.E.U. All authors have read and agreed to the published version of the manuscript.

References

1. Urquiaga, I.; Leighton, F. Plant polyphenol antioxidants and oxidative stress. *Biol. Res.* **2000**, *33*, 55–64. [CrossRef] [PubMed]
2. Fan, L.; Thompson, J.W.; Robinson, J.R. Understanding gas production mechanism and effectiveness of well stimulation in the Haynesville Shale through reservoir simulation. *Soc. Pet. Eng. Can. Unconv. Resour. Int. Pet. Conf.* **2010**, *1*, 352–366.
3. Crowe, C.; Masmonteil, J.; Thomas, R. Trends in matrix acidizing. *Oilf. Rev.* **1992**, *4*, 24–40.
4. Abdel Ghany, N.A.; Shehata, M.F.; Saleh, R.M.; El Hosary, A.A. Novel corrosion inhibitors for acidizing oil wells. *Mater. Corros.* **2017**, *68*, 355–360. [CrossRef]
5. Huizinga, S.; Liek, W.E. Corrosion behavior of 13% chromium steel in acid stimulations | Corrosion | OnePetro. *Corrosion* **1994**, *50*, NACE-94070555. [CrossRef]

6. Abd El-Lateef, H.M. Synergistic effect of polyethylene glycols and rare earth Ce^{4+} on the corrosion inhibition of carbon steel in sulfuric acid solution: Electrochemical, computational, and surface morphology studies. *Res. Chem. Intermed.* **2015**, *42*, 3219–3240. [CrossRef]

7. Singh, A.; Quraishi, M.A. Acidizing Corrosion Inhibitors: A Review. *J. Mater. Environ. Sci.* **2015**, *6*, 224–235.

8. Frenler, F.B.; Growcock, W.W.; Lopp, V.R. *Mechanisms of Corrosion Inhibitors Used in Acidizing Wells*; SPE Production Engineering: Richardson, TX, USA, 1988; pp. 584–590.

9. Zhang, J.; Sun, X.; Ren, Y.; Du, M. The synergistic effect between imidazoline-based dissymmetric bis-quaternary ammonium salts and thiourea against CO_2 corrosion at high temperature. *J. Surfactants Deterg.* **2015**, *18*, 981–987. [CrossRef]

10. Odewunmi, N.A.; Solomon, M.M.; Umoren, S.A.; Ali, S.A. Comparative studies of the corrosion inhibition efficacy of a dicationic monomer and its polymer against API X60 steel corrosion in simulated acidizing fluid under static and hydrodynamic conditions. *ACS Omega* **2020**, *5*, 27057–27071. [CrossRef]

11. Nations, U. *Globally Harmonized System of Classification and Labelling of Chemicals (GHS)*, 6th ed.; UNECE: Geneva, Switzerland, 2015; ISBN 9789211170870.

12. Alhaffar, M.T.; Umoren, S.A.; Obot, I.B.; Ali, S.A.; Solomon, M.M. Studies of the anticorrosion property of a newly synthesized green isoxazolidine for API 5L X60 steel in acid environment. *J. Mater. Res. Technol.* **2019**, *8*, 4399–4416. [CrossRef]

13. Mohammed, A.R.I.; Solomon, M.M.; Haruna, K.; Umoren, S.A.; Saleh, T.A. Evaluation of the corrosion inhibition efficacy of Cola acuminata extract for low carbon steel in simulated acid pickling environment. *Environ. Sci. Pollut. Res.* **2020**, *27*, 34270–34288. [CrossRef]

14. Umoren, S.A.; Solomon, M.M. Protective polymeric films for industrial substrates: A critical review on past and recent applications with conducting polymers and polymer composites/nanocomposites. *Prog. Mater. Sci.* **2019**, *104*, 380–450. [CrossRef]

15. Shang, Z.; Zhu, J. Overview on plant extracts as green corrosion inhibitors in the oil and gas fields. *J. Mater. Res. Technol.* **2021**, *15*, 5078–5094. [CrossRef]

16. Tan, B.; Zhang, S.; Cao, X.; Fu, A.; Guo, L.; Marzouki, R.; Li, W. Insight into the anti-corrosion performance of two food flavors as eco-friendly and ultra-high performance inhibitors for copper in sulfuric acid medium. *J. Colloid Interface Sci.* **2022**, *609*, 838–851. [CrossRef] [PubMed]

17. Tan, B.; Lan, W.; Zhang, S.; Deng, H.; Qiang, Y.; Fu, A.; Ran, Y.; Xiong, J.; Marzouki, R.; Li, W. *Passiflora edulia* Sims leaves extract as renewable and degradable inhibitor for copper in sulfuric acid solution. *Colloids Surf. A Physicochem. Eng. Asp.* **2022**, *645*, 128892. [CrossRef]

18. Supelco. Safety Data Sheet—Aspartame.

19. Aspartame—American Chemical Society. Available online: https://www.acs.org/content/acs/en/molecule-of-the-week/archive/a/aspartame.html (accessed on 20 May 2022).

20. NACE; ASTM. *ASTMG31-12a Standard Guide for Laboratory Immersion Corrosion Testing of Metals*; ASTM International: West Conshohocken, PA, USA, 2010; Volume 100.

21. Singh, A.; Caihong, Y.; Yaocheng, Y.; Soni, N.; Wu, Y.; Lin, Y. Analyses of new electrochemical techniques to study the behavior of some corrosion mitigating polymers on N80 tubing steel. *ACS Omega* **2019**, *4*, 3420–3431. [CrossRef]

22. Solomon, M.M.; Umoren, S.A.; Udosoro, I.I.; Udoh, A.P. Inhibitive and adsorption behaviour of carboxymethyl cellulose on mild steel corrosion in sulphuric acid solution. *Corros. Sci.* **2010**, *52*, 1317–1325. [CrossRef]

23. Finšgar, M.; Jackson, J. Application of corrosion inhibitors for steels in acidic media for the oil and gas industry: A review. *Corros. Sci.* **2014**, *86*, 17–41. [CrossRef]

24. Solomon, M.M.; Umoren, S.A.; Quraishi, M.A.; Tripathi, D.; Abai, E.J. Effect of akyl chain length, flow, and temperature on the corrosion inhibition of carbon steel in a simulated acidizing environment by an imidazoline-based inhibitor. *J. Pet. Sci. Eng.* **2020**, *187*, 106801. [CrossRef]

25. Key, J.A. Factors that Affect the Rate of Reactions. In *Introductory Chemistry*; Prentice Hall: Hoboken, NJ, USA, 2007.

26. Umoren, S.A.; Obot, I.B.; Ebenso, E.E.; Okafor, P.C.; Ogbobe, O.; Oguzie, E.E. Gum arabic as a potential corrosion inhibitor for aluminium in alkaline medium and its adsorption characteristics. *Anti-Corros. Methods Mater.* **2006**, *53*, 277–282. [CrossRef]

27. Khadraoui, A.; Khelifa, A. Ethanolic extract of *Ruta chalepensis* as an eco-friendly inhibitor of acid corrosion of steel. *Res. Chem. Intermed.* **2013**, *39*, 3937–3948. [CrossRef]

28. Abdulazeez, I.; Al-Hamouz, O.C.S.; Khaled, M.; Al-Saadi, A.A. Inhibition of mild steel corrosion in CO_2 and H_2S-saturated acidic media by a new polyurea-based material. *Mater. Corros.* **2020**, *71*, 646–662. [CrossRef]

29. Wang, X.; Li, L.; Xie, Z.H.; Yu, G. Duplex coating combining layered double hydroxide and 8-quinolinol layers on Mg alloy for corrosion protection. *Electrochim. Acta* **2018**, *283*, 1845–1857. [CrossRef]

30. Jing, C.; Wang, Z.; Gong, Y.; Huang, H.; Ma, Y.; Xie, H.; Li, H.; Zhang, S.; Gao, F. Photo and thermally stable branched corrosion inhibitors containing two benzotriazole groups for copper in 3.5 wt% sodium chloride solution. *Corros. Sci.* **2018**, *138*, 353–371. [CrossRef]

31. Azghandi, M.V.; Davoodi, A.; Farzi, G.A.; Kosari, A. Corrosion inhibitive evaluation of an environmentally friendly water-base acrylic terpolymer on mild steel in hydrochloric acid media. *Metall. Mater. Trans. A Phys. Metall. Mater. Sci.* **2013**, *44*, 5493–5504. [CrossRef]

32. Leng, Y.; Qi, H. Solubility of aspartame in water, methanol, ethanol and different binary mixtures in the temperature range of (278.15 to 333.15) K. *J. Chem. Eng. Data* **2014**, *59*, 1549–1555. [CrossRef]

33. Gamry.com Basics of EIS: Electrochemical Research-Impedance. Available online: https://www.gamry.com/application-notes/EIS/basics-of-electrochemical-impedance-spectroscopy (accessed on 8 May 2022).

34. Öztürk, S.; Gerengi, H.; Solomon, M.M.; Gece, G.; Yıldırım, A.; Yıldız, M. A newly synthesized ionic liquid as an effective corrosion inhibitor for carbon steel in HCl medium: A combined experimental and computational studies. *Mater. Today Commun.* **2021**, *29*, 102905. [CrossRef]

35. Srikanth, A.P.; Sunitha, T.G.; Raman, V.; Nanjundan, S.; Rajendran, N. Synthesis, characterization and corrosion protection properties of poly(N-(acryloyloxymethyl) benzotriazole-co-glycidyl methacrylate) coatings on mild steel. *Mater. Chem. Phys.* **2007**, *103*, 241–247. [CrossRef]

36. Solomon, M.M.; Umoren, S.A.; Quraishi, M.A.; Salman, M. Myristic acid based imidazoline derivative as effective corrosion inhibitor for steel in 15% HCl medium. *J. Colloid Interface Sci.* **2019**, *551*, 47–60. [CrossRef]

37. Qiang, Y.; Zhang, S.; Tan, B.; Chen, S. Evaluation of Ginkgo leaf extract as an eco-friendly corrosion inhibitor of X70 steel in HCl solution. *Corros. Sci.* **2018**, *133*, 6–16. [CrossRef]

38. Corrales-Luna, M.; Le Manh, T.; Romero-Romo, M.; Palomar-Pardavé, M.; Arce-Estrada, E.M. 1-Ethyl 3-methylimidazolium thiocyanate ionic liquid as corrosion inhibitor of API 5L X52 steel in H$_2$SO$_4$ and HCl media. *Corros. Sci.* **2019**, *153*, 85–99. [CrossRef]

39. Palomar-Pardavé, M.; Romero-Romo, M.; Herrera-Hernández, H.; Abreu-Quijano, M.A.; Likhanova, N.V.; Uruchurtu, J.; Juárez-García, J.M. Influence of the alkyl chain length of 2 amino 5 alkyl 1, 3, 4 thiadiazole compounds on the corrosion inhibition of steel immersed in sulfuric acid solutions. *Corros. Sci.* **2012**, *54*, 231–243. [CrossRef]

40. Sedik, A.; Lerari, D.; Salci, A.; Athmani, S.; Bachari, K.; Gecibesler, H.; Solmaz, R. Dardagan Fruit extract as eco-friendly corrosion inhibitor for mild steel in 1 M HCl: Electrochemical and surface morphological studies. *J. Taiwan Inst. Chem. Eng.* **2020**, *107*, 189–200. [CrossRef]

41. Zhang, D.Q.; Gao, L.X.; Zhou, G.D. Inhibition of copper corrosion by bis-(1-benzotriazolymethylene)-(2,5-thiadiazoly)-disulfide in chloride media. *Appl. Surf. Sci.* **2004**, *225*, 287–293. [CrossRef]

42. Gerengi, H.; Mielniczek, M.; Gece, G.; Solomon, M.M. Experimental and Quantum Chemical Evaluation of 8-Hydroxyquinoline as a Corrosion Inhibitor for Copper in 0.1 M HCl. *Ind. Eng. Chem. Res.* **2016**, *55*, 9614–9624. [CrossRef]

43. Solomon, M.M.; Gerengi, H.; Umoren, S.A. Carboxymethyl cellulose/silver nanoparticles composite: Synthesis, characterization and application as a benign corrosion inhibitor for St37 steel in 15% H$_2$SO$_4$ medium. *ACS Appl. Mater. Interfaces* **2017**, *9*, 6376–6389. [CrossRef]

44. de Araújo Macedo, R.G.M.; do Nascimento Marques, N.; Tonholo, J.; de Carvalho Balaban, R. Water-soluble carboxymethylchitosan used as corrosion inhibitor for carbon steel in saline medium. *Carbohydr. Polym.* **2019**, *205*, 371–376. [CrossRef]

45. Ghelichkhah, Z.; Dehkharghani, F.K.; Sharifi-Asl, S.; Obot, I.B.; Macdonald, D.D.; Farhadi, K.; Avestan, M.S.; Petrossians, A. The inhibition of type 304LSS general corrosion in hydrochloric acid by the New Fuchsin compound. *Corros. Sci.* **2021**, *178*, 109072. [CrossRef]

46. Aljourani, J.; Raeissi, K.; Golozar, M.A. Benzimidazole and its derivatives as corrosion inhibitors for mild steel in 1 M HCl solution. *Corros. Sci.* **2009**, *51*, 1836–1843. [CrossRef]

47. Casaletto, M.P.; Figà, V.; Privitera, A.; Bruno, M.; Napolitano, A.; Piacente, S. Inhibition of Cor-Ten steel corrosion by "green" extracts of Brassica campestris. *Corros. Sci.* **2018**, *136*, 91–105. [CrossRef]

48. Sangeetha, Y.; Meenakshi, S.; Sundaram, C.S. Interactions at the mild steel acid solution interface in the presence of O-fumaryl-chitosan: Electrochemical and surface studies. *Carbohydr. Polym.* **2016**, *136*, 38–45. [CrossRef] [PubMed]

49. Mathew, Z.P.; Rajan, K.; Augustine, C.; Joseph, B.; John, S. Corrosion inhibition of mild steel using poly (2-ethyl -2-oxazoline) in 0.1 M HCl solution. *Heliyon* **2020**, *6*, e05560. [CrossRef] [PubMed]

50. Subramania, A.; Sathiya Priya, A.R.; Muralidharan, V.S. Development of novel acidizing inhibitors for carbon steel corrosion in 15% boiling hydrochloric acid. *Corrosion* **2008**, *64*, 687.

51. Haruna, K.; Obot, I.B.; Ankah, N.K.; Sorour, A.A.; Saleh, T.A. Gelatin: A green corrosion inhibitor for carbon steel in oil well acidizing environment. *J. Mol. Liq.* **2018**, *264*, 515–525. [CrossRef]

52. Kowsari, E.; Payami, M.; Amini, R.; Ramezanzadeh, B.; Javanbakht, M. Task-specific ionic liquid as a new green inhibitor of mild steel corrosion. *Appl. Surf. Sci.* **2014**, *289*, 478–486. [CrossRef]